

RESEARCH LETTER

10.1029/2018GL077830

Key Points:

- Vegetation-climate interactions are implemented in a regional Earth system model
- The spatiotemporal patterns of biogeophysical feedbacks associated with ecosystem responses to future Arctic climate change are quantified
- Biogeophysical feedbacks modulate the future Arctic climate conditions amenable to a continuation and enhancement of current greening trends

Supporting Information:

- Supporting Information S1

Correspondence to:

W. Zhang,
wenxin@ign.ku.dk

Citation:

Zhang, W., Miller, P. A., Jansson, C., Samuelsson, P., Mao, J., & Smith, B. (2018). Self-amplifying feedbacks accelerate greening and warming of the Arctic. *Geophysical Research Letters*, 45, 7102–7111. <https://doi.org/10.1029/2018GL077830>

Received 8 MAR 2018

Accepted 29 JUN 2018

Accepted article online 5 JUL 2018

Published online 20 JUL 2018

Self-Amplifying Feedbacks Accelerate Greening and Warming of the Arctic

W. Zhang^{1,2} , P. A. Miller¹ , C. Jansson³, P. Samuelsson³, J. Mao⁴ , and B. Smith¹ 

¹Department of Physical Geography and Ecosystem Science, Lund University, Lund, Sweden, ²Center for Permafrost (CENPERM), Department of Geosciences and Natural Resource Management, University of Copenhagen, Copenhagen, Denmark, ³Rosby Centre, Swedish Meteorological and Hydrological Institute, Norrköping, Sweden, ⁴Environmental Sciences Division and Climate Change Science Institute, Oak Ridge National Laboratory, Oak Ridge, TN, USA

Abstract Increased greening, higher vegetation productivity, and shrubification have been observed in Arctic tundra in response to recent warming. Such changes have affected the near-surface climate through opposing biogeophysical feedbacks (BF) associated with changes to albedo and evapotranspiration. However, the likely spatiotemporal variations of BF to future climate change and the consequences for Arctic vegetation and ecology have not been robustly quantified. We apply a regional Earth system model (RCA-GUESS) interactively coupling atmospheric dynamics to land vegetation response in three potential 21st-century radiative forcing simulations for the Arctic. We find that BF, dominated by albedo-mediated warming in early spring and evapotranspiration-mediated cooling in summer, have the potential to amplify or modulate local warming and enhance summer precipitation over land. The magnitude of these effects depends on radiative forcing and subsequent ecosystem responses. Thus, it is important to account for BF when assessing future Arctic climate change and its ecosystem impacts.

Plain Language Summary Arctic terrestrial ecosystems are in a state of transition due to their responses to rapid warming observed in recent decades. The changes in distribution and composition of terrestrial ecosystems may induce biogeophysical feedbacks that modulate the Arctic climate. Few studies, however, have quantified the impacts of such feedbacks by accounting for the tight coupling between physical forcing factors and transient vegetation responses to the evolving climate. Using a fully coupled regional Earth system model (RCA-GUESS), we discern impacts of biogeophysical feedbacks on regional climates at various levels of radiative forcing. We find that feedbacks dominated by albedo-mediated warming in early spring and evapotranspiration-mediated cooling in summer can strongly alter the future AC changes. This study indicates that biogeophysical interactions between the Arctic climate and land vegetation may shift seasonal profiles of temperature and precipitation, and should be taken into account in future assessments of climate change and its impacts in the Arctic.

1. Introduction

The structure, functioning, and composition of the Arctic's terrestrial ecosystems are currently in a state of transition due to their responses to ongoing climate change (ACIA, 2005; Elmendorf et al., 2012; Tape et al., 2006). Biogeophysical feedbacks (BF) induced by changes in the distribution and composition of terrestrial ecosystems, such as increased leaf cover, tundra shrubification, and treeline advance, may alter energy, water, and momentum across the land-atmosphere boundary, modulating the evolution of climate over various temporal and spatial scales (Claussen et al., 2006; Li et al., 2015; Willeit et al., 2014). BF, manifested at regional scales, directly change local climate conditions and further affect the net CO₂ exchange of the biosphere (Green et al., 2017; Li et al., 2015; Zhang et al., 2014). In the taiga-tundra transition zones, positive BF to near-surface warming are triggered by a reduction of albedo associated with the land surface darkening due to denser, taller, northward- and upward-expanding woody vegetation and changes in the extent and duration of snow cover (Chapin et al., 2005; Lorant et al., 2013). Meanwhile, ecosystems with higher leaf area index (LAI) and lower surface canopy resistance can potentially promote more efficient transport of water vapor to the atmosphere, leading to negative BF to near-surface warming (Bonan, 2008; Göttel et al., 2008). Therefore, BF-induced changes in the regional climate are contingent upon how ecosystems respond to future climate change and fertilization by atmospheric CO₂. Based on observed relationships between biotic distribution and abiotic variables, Pearson et al. (2013) estimate how two opposing BF mechanisms, namely, albedo-mediated feedback and evapotranspiration (ET)-mediated feedback, might evolve under

future shifts in Arctic vegetation. They conclude that the overall feedback induced by vegetation changes is positive and may cause greater warming than previous predictions. Such studies, however, only address the BF impacts by estimating potential changes in surface atmospheric heating and do not consider the tight coupling between physical forcing factors and transient ecosystem dynamics.

Models contributing to the Coupled Model Intercomparison Project Phase 5 (CMIP5) suggest that annual precipitation in northern high latitudes will likely increase by more than 50% this century (Bintanja & Selten, 2014; Stocker et al., 2013). This increase is attributed to intensified local evaporation and latent heat flux (LHF) over both land and sea. The greatest LHF increase over land is found in regions, such as Arctic tundra and boreal forests, believed to be most likely to experience sizeable changes (Bond-Lamberty, 2013; Dirmeyer et al., 2013; Zhang et al., 2013). This motivates an assessment of future climate evolution including BF associated with changes in the magnitude and seasonal distribution of albedo and ET.

In this study, we simulate the joint evolution of climate and vegetation across the Arctic under an ensemble of Representative Concentration Pathway (RCP) scenarios bracketing anticipated radiative forcing for the 21st century using a regional Earth system model, RCA-GUESS (Smith et al., 2011). The model accounts for an interactive coupling between physical climate processes and ecosystem processes (e.g., growth, establishment, and mortality for both woody and herbaceous species). Uniquely among available model-based studies of Arctic climate change (e.g., Göttel et al., 2008; Matthes et al., 2012; Pearson et al., 2013; Swann et al., 2010), this study focuses on detailed and transient responses of Arctic ecosystems to ongoing climate change and rises in atmospheric CO₂ concentration, accounting for legacy and lagged effects of vegetation structural and compositional changes. The model is applied at a horizontal resolution of 0.44° × 0.44°, sufficient to resolve topography and climatic gradients critical for the displacement and migration of ecotones, such as the taiga-tundra boundary, where vegetation is most rapidly changing, thus capturing local-to-regional shifts in land surface properties and the resultant effects on climate (Zhang et al., 2013). Global ESMs incorporating interactive vegetation dynamics are insufficient for the purposes of such a study, as they typically operate on resolutions too coarse to resolve surface heterogeneities (e.g., topographical complexity, physiography, and coastlines) crucial to the representation of small-scale circulation features (Kueppers et al., 2005) or tree-line dynamics (Lorant et al., 2013). Specifically, we (1) assess how well the model simulates historical seasonal variations of ecosystem-specific albedo and ET; (2) quantify BF-induced changes in 2 m air temperature and precipitation, and the relative importance of albedo- and ET-mediated feedbacks under different magnitudes of large-scale radiative forcing encapsulated by the RCPs; and (3) attribute BF to potential ecosystem responses in different subregions across the pan-Arctic land area.

2. Materials and Methods

We employed RCA-GUESS, which couples the land surface scheme of the Rossby Centre regional atmosphere model version 4 (RCA4; Kjellström et al., 2005; Samuelsson et al., 2015) with a process-based dynamic vegetation and ecosystem biogeochemistry model (LPJ-GUESS; Smith et al., 2001). RCA4 was developed from a numerical weather prediction model (HIRLAM; Undén et al., 2002) and applied to dynamically downscale the general circulation model (GCM) outputs to regional scales. Sea ice is accounted for in RCA via sea surface temperature and sea-ice cover fraction from the forcing model (i.e., ERA-Interim or a GCM). The ice temperature is prognostic using a very simple heat-transfer scheme for a predefined sea-ice thickness (Samuelsson et al., 2011; Samuelsson et al., 2015). In this study, RCA4 was applied to the CORDEX-Arctic domain, which was specified by the Coordinated Regional Climate Downscaling Experiment framework (<http://wcrp-cordex.ipsl.jussieu.fr/>). The domain covered 150 × 156 rotated longitude-latitude coordinates at a resolution of 0.44° (approximately 50 km) and 40 vertical model levels. LPJ-GUESS is an individual-based ecosystem model that explicitly represents vegetation structure, population dynamics, and resource competition among woody species and a herbaceous understory. Six plant functional types (PFTs; i.e., boreal needle-leaved evergreen trees, boreal shade-intolerant needle-leaved evergreen trees, boreal needle-leaved summer-green trees, temperate broad-leaved deciduous trees, shade-intolerant broad-leaved summer-green trees, and C3 grass) representing boreal and arctic ecosystems were parameterized (Table S1 in the supporting information). In the coupling scheme, LPJ-GUESS provides RCA4 with the daily LAI and annual cover fraction of forest land and open land to calculate turbulent fluxes based on canopy resistance, surface roughness length, and grid-averaged albedo. In turn, RCA4 provides LPJ-GUESS with daily air

temperature, precipitation, and incoming shortwave radiation to simulate vegetation dynamics and ecosystem biogeochemistry.

RCA4 used outputs from CMIP5 simulations with the EC-Earth (Hazeleger et al., 2012) as lateral forcing fields for simulations across the pan-Arctic regional domain. Separate model experiments were performed based on forcing under the RCP2.6, RCP4.5, and RCP8.5 scenarios. For each scenario, simulations with and without vegetation-atmosphere feedbacks enabled in RCA-GUESS were conducted, allowing the effects of BF to be inferred as the difference between the feedback and nonfeedback experiments. For 1961–1990, the model ran with interactive vegetation dynamics. For 1991–2100, the nonfeedback experiments ran with fixed vegetation properties averaged over the 1961–1990 period, while the feedback experiments ran with interactive vegetation dynamics for the entire scenario period. Two spin-ups of the coupled model were required to give reasonable initial states for vegetation structure and composition, carbon (C) pools and climate conditions appropriate to the 1961–1990 period. In the nonfeedback experiment, fixed vegetation properties averaged from the outputs for 1961–1990 were provided to the atmospheric part of the model throughout the future part of the run. Following the procedure described in detail by Zhang et al. (2014), both the feedback and nonfeedback runs were initialized from an off-line spin-up driven by the observation-based data set (CRU TS3.0; Mitchell & Jones, 2005) to give reasonable initial vegetation distributions and C pools, followed by a coupled spin-up for 1961–1990 to give reasonable initial climate conditions in 1990. The detailed spin-up protocol is described by Zhang et al. (2014).

The seasonal and spatial variability in albedo and LHF were evaluated for regions dominated by present-day distributions of four ecosystem types (i.e., evergreen forests, deciduous forests, mixed forests, and herbaceous vegetation) according to the ISLSCP II Potential Natural Vegetation Cover data set (Ramankutty et al., 2010; Figure S1). To evaluate the simulated albedo, the 0.5° white sky albedo from the Global Albedo Product “Globalbedo” based on the monthly average of 1998–2011 was used (Muller et al., 2012). To evaluate the simulated LHF, the 0.5° upscaled FLUXNET observation data set based on the monthly average for 1982–2011 was used (Jung et al., 2011). To illustrate the relative importance of the albedo and ET feedbacks for near-surface warming in all three RCPs, we calculated Pearson’s correlation coefficient between the respective changes in temperature (ΔT) and albedo ($\Delta\alpha$), and between ΔT and change in LHF (ΔLHF) based on their time series from 2006 to 2100 for spring (March to May) and summer (June to August). Because these two correlation coefficients have opposite signs, we sum the calculated correlation coefficients, obtaining a metric between -1 and 1 . 1 or -1 indicates the perfect correlation. Positive values reflect the extent to which ET-induced feedback dominates the total feedback-induced changes in temperature, while negative values scale with the dominant contribution of albedo-induced feedback. To investigate in more detail how BF in different scenarios are dependent on ecosystem responses to potential future climate change, we selected six subregions (i.e., Scandes Mountains [SM], West Siberia [WS], East Siberia [ES], Far East Siberia [FS], Alaska [AL], and North Canada [NC]; see Figure S2) for a closer analysis.

3. Results

The model captured the observed, ecosystem-specific seasonal variation in albedo and LHF (Figure 1). However, the model exhibited a larger spatial variability (indicated by error bars) than the observations. For LHF, the greatest disagreement with observations was found over regions identified as mixed forests and herbaceous vegetation, where the model underestimated LHF by 5–15 W/m^2 in May to August (Figures 1c and 1d). Considering their spatial variations, the observations in general were within the variations in the model estimates. For albedo, the model matched the observed values in June to September in all ecosystems. However, the model overestimated albedo in October to December over deciduous forests, mixed forests, and herbaceous vegetation (Figures 1b–1d). Compared to 1961–1990, the projections (2071–2100) resulted in an increase (5–15 W/m^2) of LHF in spring and summer (Figure S3). The most pronounced increase of LHF was found in summer under RCP8.5. The spring albedo for 2071–2100 was found to decrease by 0.2 relative to 1961–1990 over mountainous regions (Figures S4a–S4c). The changes in summer albedo were effected by a denser vegetative cover and an increased deciduous forest fraction, resulting in a reduction around 0.05–0.15 depending on the RCP scenario (Figures S4d–S4f and S5d–S5f). The largest reduction in albedo in summer under RCP8.5 was seen in the subregion FS, coincident with the dominant species of trees changing from evergreen to deciduous (Figures S4f and S5f).

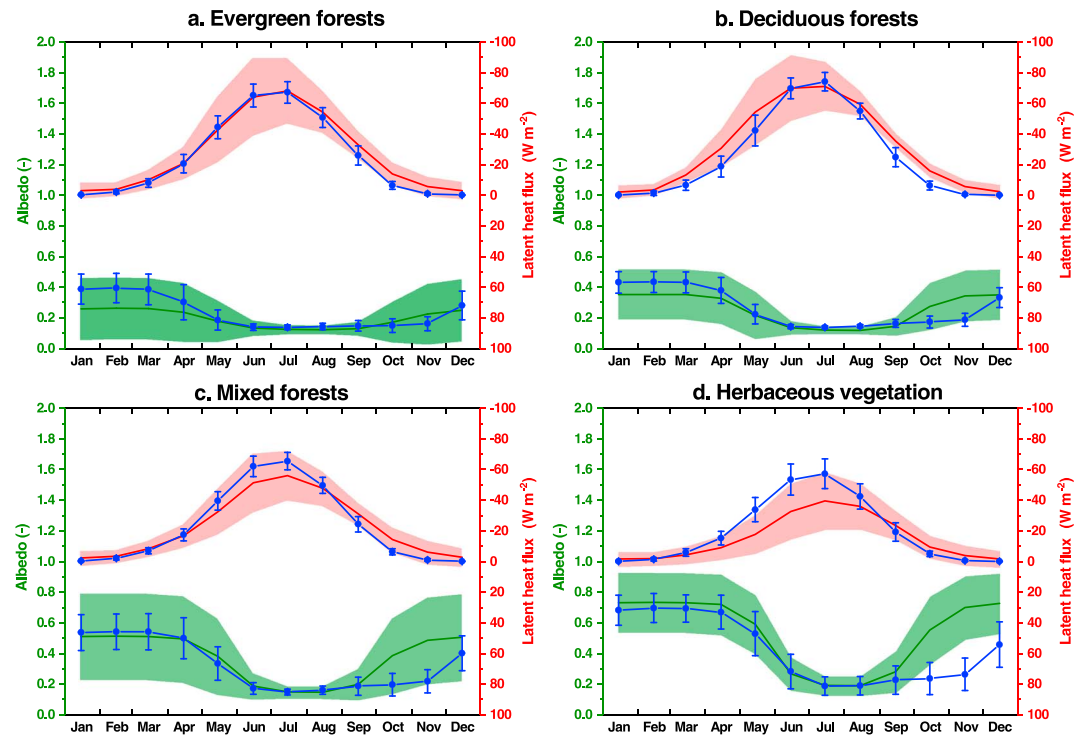


Figure 1. Seasonal variations of albedo and latent heat fluxes for four ecosystem types (a) evergreen forests, (b) deciduous forests, (c) mixed forests, and (d) herbaceous vegetation. The red and green colors denote the model estimates. The blue color denotes the observational data sets (i.e., the 0.5° white sky albedo from the Global Albedo Product “Globalbedo” based on the monthly average of 1998–2011, Muller et al., 2012, and the 0.5 degree upscaled FLUXNET observations of latent heat flux data set based on the monthly average of 1982–2011; Jung et al., 2011). Error bars represent one standard deviation of the data set for grid cells belonging to each ecosystem type.

Reflecting the nonlinear and lagged response of vegetation structure and function to climate change, the BF-induced changes in 2 m air temperature in the subregions analyzed here varied in sign, magnitude, and by season in the late 21st century and did not merely show a proportional response to the level of radiative forcing (Figure 2). For instance, winter and spring of WS and summer of ES and FS experienced a higher warming in RCP4.5 than in RCP2.6, but a lower warming in RCP8.5 than in RCP4.5. In contrast, increased or decreased warming monotonically followed the increase of prescribed radiative forcing (e.g., autumn over ES and WS and spring and summer over SM and NC). In contrast to the responses seen in 2 m air temperature, the spatial patterns of BF-induced changes in precipitation were similar across all RCPs (Figure 3). A larger increase in precipitation was found in summer in mountainous regions and WS. Furthermore, the higher the level of radiative forcing, the higher the BF-induced increase in precipitation.

Averaged across land areas, self-amplifications in both 2 m air temperature and precipitation were found (Figure 4). The slopes of the linear regression for BF-induced changes in 2 m air temperature were 0.35 °C per century (RCP2.6), 0.39 °C per century (RCP4.5), and 0.25 °C per century (RCP8.5; Figure 4a). The much lower slope in RCP 8.5 was due to the decline in the temperature increase towards the end of the century, which even returned to zero by 2100 (Figure 4a). The seasonal profile of temperature change showed the most pronounced increased warming (RCP2.6: 1.27 °C/month, RCP4.5: 1.39 °C/month, and RCP8.5: 1.42 °C/month) occurring in spring (March to May; Figure 4b). BF-induced cooling was also noted in July to October, leading to temperature decreases of -0.13 °C/month (RCP2.6), -0.3 °C/month (RCP4.5), and -0.51 °C/month (RCP8.5). BF-induced changes in precipitation displayed consistent patterns in all RCPs, with (linear) trends of 6.7 mm per century (RCP2.6), 7.7 mm per century (RCP4.5), and 9.6 mm per century (RCP8.5), indicative of a regionally intensified hydrological cycle (Figure 4c). In summer, precipitation increased in magnitude and variability as radiative forcing increased (Figure 4d). The most marked variations in RCP8.5 indicated more years of drier or wetter summers.

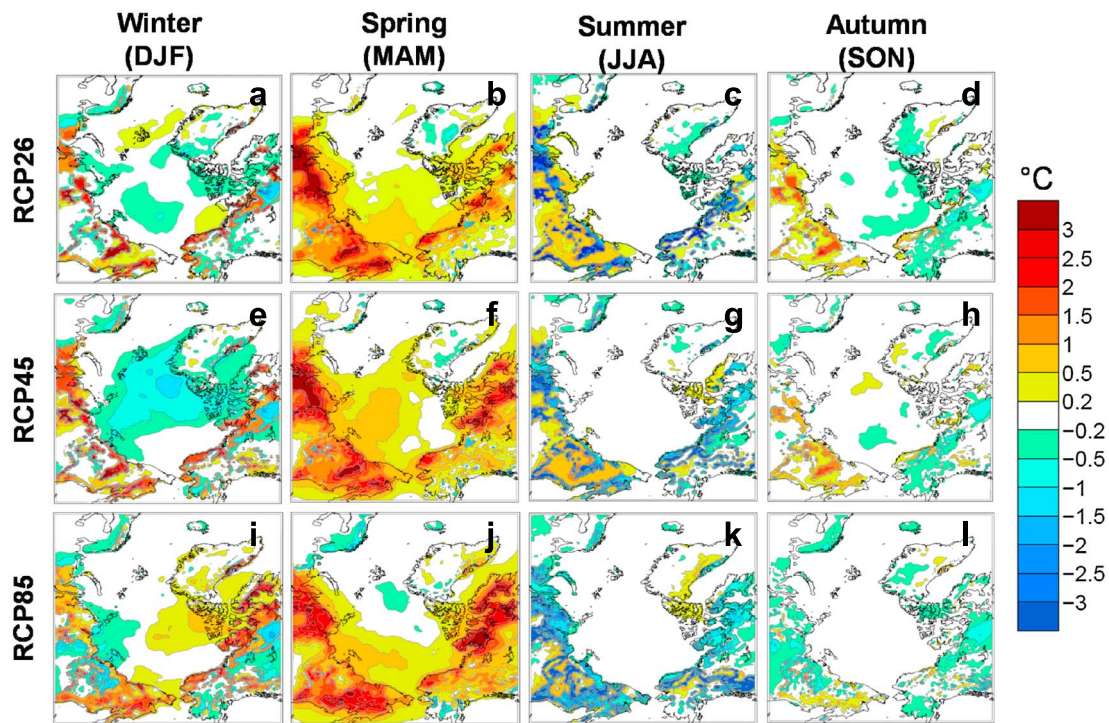


Figure 2. Changes in 2 m air temperature (°C) due to biogeophysical feedbacks for 2071–2100 in different seasons (columns) under different RCP scenarios (rows) across the CORDEX-Arctic domain (the Arctic domain in the Coordinated Regional Climate Downscaling Experiment Framework; <http://wcrp-cordex.ipsl.jussieu.fr/index.php/community/domain-arctic-cordex>). RCP = Representative Concentration Pathway.

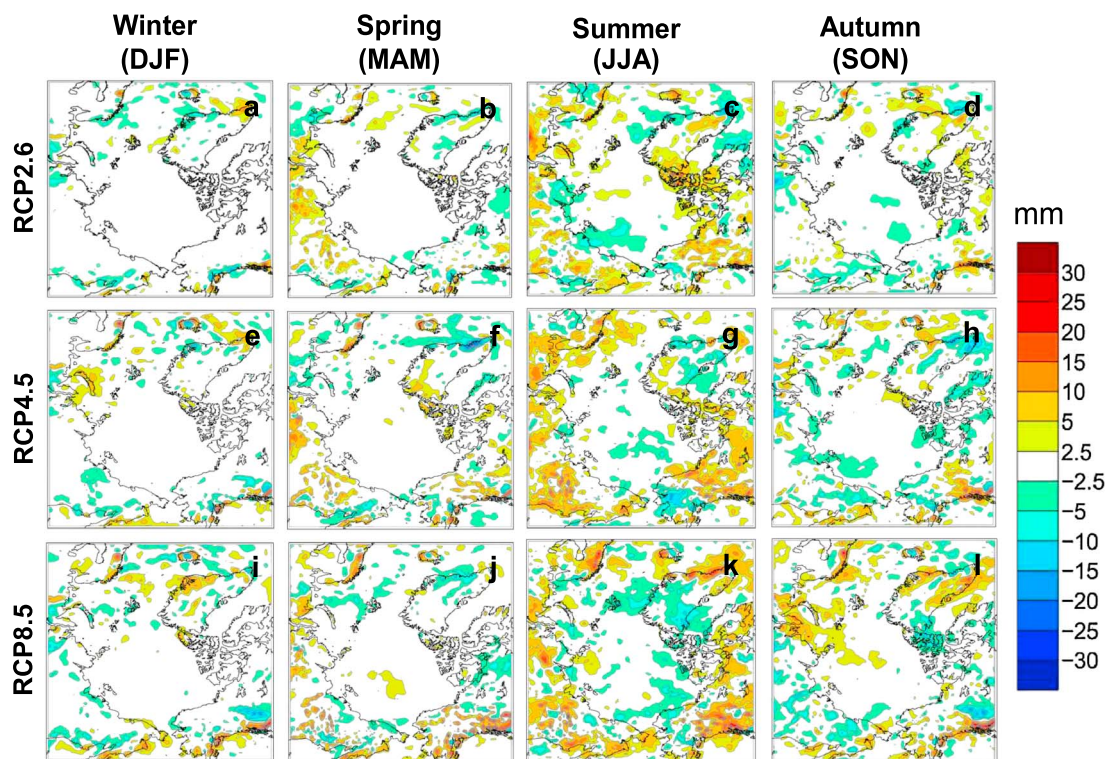


Figure 3. Changes in precipitation (mm/month) due to biogeophysical feedbacks for 2071–2100 in different seasons (columns) under different RCP scenarios (rows) across the CORDEX-Arctic domain.

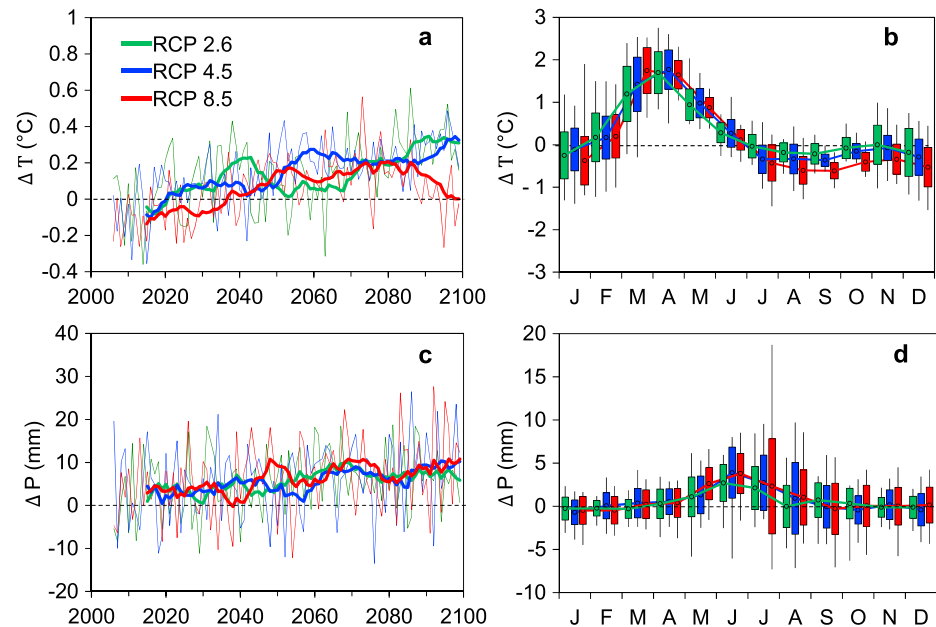


Figure 4. The interannual and seasonal variations (2071–2100) of changes in temperature (°C) and precipitation (mm) due to biogeophysical feedbacks under different RCP scenarios. In (a) and (c), the bold lines show 10-year moving averages and the thin lines show interannual variation. In (b) and (d), each box plot shows the mean (dot), one standard deviation range (colored shading), and maximum and minimum values (whiskers) for all the grid cells in the CORDEX-Arctic domain.

Spatial patterns of relative importance for the albedo-mediated feedback and ET-mediated feedback to determine near-surface warming showed that in spring, the albedo-mediated feedback played an increasingly important role in effecting increased warming in the higher RCP scenarios across most land areas, except in ES where the albedo-mediated feedback was gradually offset by the ET-mediated feedback (Figures 5a–5c). In summer, the ET-mediated feedback tends to become increasingly stronger (Figures 5d–5f) as the radiative forcing is increased. The most marked ET-mediated feedback was seen along mountain ranges and regions presently occupied by Arctic tundra. These patterns are related to different extents of subregional ecological resilience to climate change (Figure S6). According to the temporal variations for each PFT's fractional LAI, the largest compositional change in vegetation species was found in NC, WS, ES, and FS. For instance, boreal forests in WS and ES exhibited a shift from dominance by deciduous (larch) to evergreen (pine and spruce) conifer species. Encroachment by broad-leaved deciduous species into Arctic tundra was increasingly apparent in NC and FC in the higher RCPs. Such shifts were invoked by the crossing of temperature thresholds for establishment and survival of trees (e.g., earlier spring zero-degree crossing dates, changes to the number of annual growing degree-days, annual temperature, and seasonality changes), and these thresholds were reached earlier and over a larger portion of the Arctic land area in the strongest forcing scenario (Figure S7). In contrast, changes in SM and AL were rather modest, implying a higher subregional ecological resilience, apparent as an increase of LAI for all the species but a relatively stable composition.

4. Discussion

The model in general captures seasonal variations of ecosystem-specific LHF and albedo, though mismatches between the simulations and observations indicate room for further model improvement. For instance, the main underestimation of LHF is found in herbaceous vegetation in May–July, which is the period of substantial snowmelt. However, as the observations are upscaled from the FLUXNET data sets, which contain very few measurements from Arctic tundra, more observations are required to determine how well the model captures the process of snowmelt. The mismatch of albedo shown in mixed forests and herbaceous vegetation in October to December is largely related to snow processes and precipitation in RCA4. Previous studies

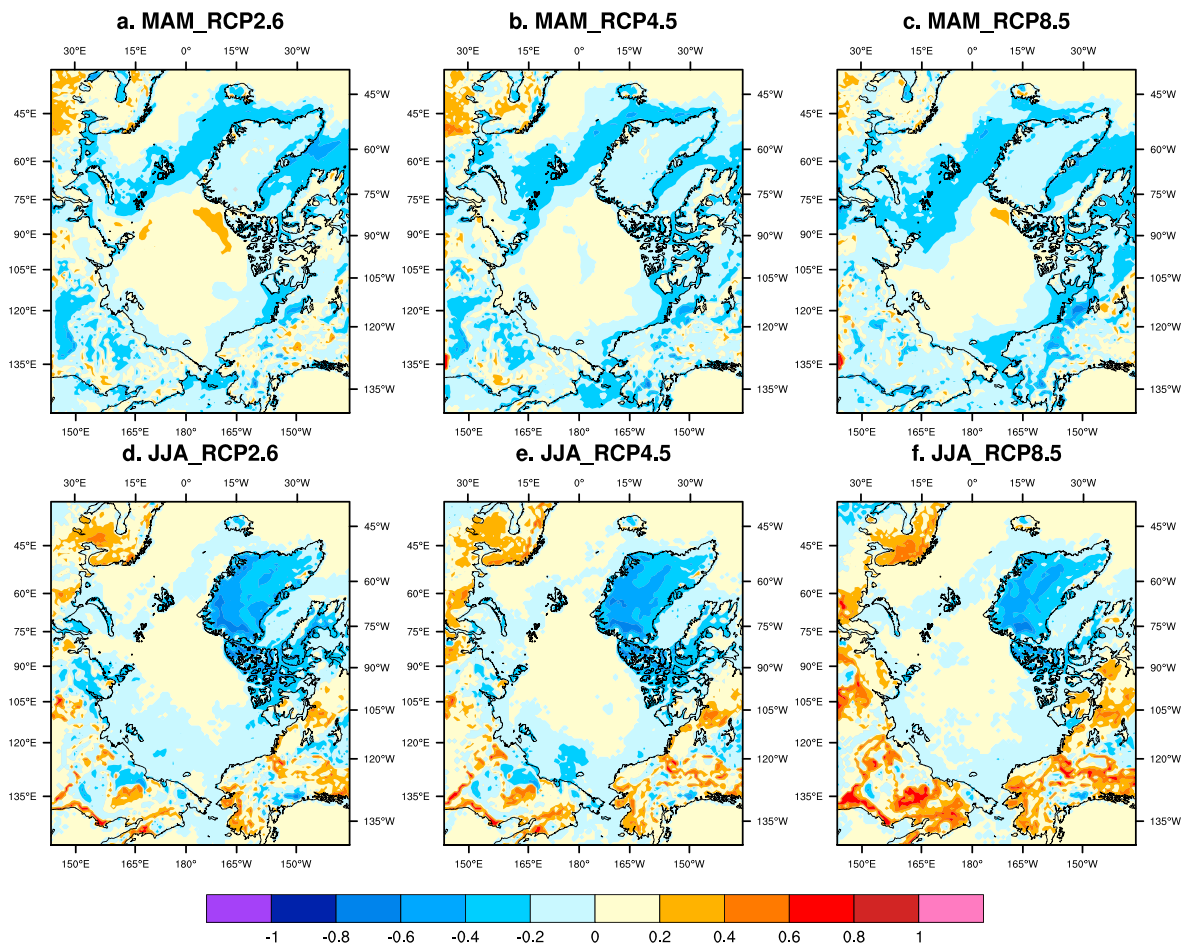


Figure 5. The relative importance of albedo feedback and evapotranspiration feedbacks to near-surface warming under different RCP scenarios in spring ((a)–(c) March to May) and summer ((d)–(f) June to August). The relative importance was quantified by summing up Pearson’s correlation coefficient for albedo changes and near-surface warming and Pearson’s correlation coefficient for latent heat flux change and near-surface warming. The index shown ranges from -1 to 1 , where -1 represents a perfect correlation between albedo change and warming change, $+1$ represents a perfect correlation between LHF change and warming change, and 0 signifies no correlation.

(e.g., Samuelsson et al., 2011; Wyser et al., 2008) argued that the effect of snow aging processes on albedo might be too weak in RCA, and precipitation might be too frequent in mountainous areas where mixed forests and Arctic tundra were located. This led to the overall surface albedo being closer to the prognostic snow albedo over open land, normally ranging from 0.6 to 0.85. Moreover, snow redistribution due to wind is an important factor in determining albedo during the snow season. This is not accounted for in the current model setup.

The future changes (2071–2100 relative to 1961–1990) of albedo and LHF are comparable to estimates from previous studies. For instance, the albedo decline in the lower RCP scenarios is close to the estimate of Chapin et al. (2005), that is, an albedo reduction of approximately 0.06 resulting from a complete conversion of tundra to forest in the postsnowmelt season. Euskirchen et al. (2009) used a terrestrial ecosystem model driven with climate fields generated from three GCMs (CSIRO2, HadCM3, and PCM) following the IPCC Special Report: Emissions Scenarios (SRES) A2 scenario to estimate the maximum decline in summer albedo, which was approximately 0.02 in Alaska. In our simulations, the BF-induced decline in albedo in Alaska was 0.05 to 0.1 in the RCP8.5 simulation. Bonfils et al. (2012) used the Community Climate System Model version 4 following an RCP8.5 scenario and estimated the difference in the summertime LHF between ecosystems dominated by tall and short shrubs to be about 7.5 W/m^2 . Moreover, an uncoupled simulation using the Arctic-enabled version of LPJ-GUESS adopting tall and low shrubs, arctic open-ground vegetation, and

wetland PFTs estimated changes in summertime LHF for a similar time window to be 4–5 W/m² for the SRES A1B forcing scenario (Zhang et al., 2013).

Arctic tundra and parts of the boreal forest have been found to be sensitive to recent climate variability, indicating that such ecosystems may cross a threshold to an alternative state when perturbed by environmental change (Dekker et al., 2010; Seddon et al., 2016). Analysis of satellite data has suggested that the biophysical effects of boreal forests on local climate are moderate cooling in summer and moderate warming in winter, with net warming on an annual scale, although satellite data cannot measure feedbacks (Alkama & Cescatti, 2016; Li et al., 2015). These effects are mainly driven by the competing seasonal effects of ET and albedo, indicating an enhanced hydrological cycling. Our simulations are in line with extensive observational evidence suggesting that CO₂ fertilization and warming over a prolonged growing season can increase vegetation and leaf cover, intensify competition between deciduous and evergreen trees, and promote an expansion of trees and shrubs into tundra areas. Our findings complement observational studies—which can infer but not explicitly isolate the operation of feedback mechanisms—by demonstrating that such shifts in vegetation structure and composition feed back to the regional climate, resulting in pronounced shifts in temperature and precipitation patterns and seasonality. The character and strength of the feedbacks simulated by our model largely agree with estimates based on previous studies of tundra-forest transitions (e.g., Beringer et al., 2005; Berner et al., 2013; De Wit et al., 2014; Wramneby et al., 2010).

Woody species play a pivotal role in regulating the surface exchange of energy and water vapor, determining the strength of land surface-atmosphere coupling (Bonan, 2008; Zhang et al., 2013). A large decline of albedo across boreal forests and Arctic tundra in spring, as a unique feature of northern high latitudes, enhances surface warming by increasing atmospheric heating (Figures S3 and S8), subsequently affecting snow dynamics (Lorant et al., 2013) and photosynthetic activity. In spite of phenological changes driven by an earlier spring-onset of photosynthesis, the lower albedo causes a larger increase in sensible heat flux than the associated increase in LHF (higher Bowen ratio; Beringer et al., 2005; Figure S9), resulting in net warming. In summer, the changes in day length and precipitation, and shifts in ecosystem types (from tundra to forests) or phenology (from evergreen to deciduous) determine the partitioning of the land-atmosphere energy flux and generally lower the Bowen ratio, resulting in extra summer cooling. Although albedo is also reduced in summer, lower insolation owing to increased cloudiness may largely compensate for the increased radiation absorbed by the surface. Relative to Arctic tundra, boreal forests are characterized by a stronger coupling of the surface to the atmosphere, manifested as larger turbulent heat fluxes in summer (Kasurinen et al., 2014; Matthes et al., 2012). An increased woody cover may further intensify vegetative transpiration, leading to reduced atmospheric stability and enhanced convective precipitation (Zhang & Walsh, 2006).

The version of LPJ-GUESS used for this study does not account for the processes of permafrost thawing and nitrogen cycling, which however may be critical in determining the full extent of BF to climate. Permafrost thawing significantly alters land surface energy partitioning, depending on whether ecosystems are dry or wet and the extent of thawing (Lawrence et al., 2015; Stiegler et al., 2016). Vegetation, in turn, can reinforce thawing due to albedo-induced warming (Lawrence & Swenson, 2011) or alleviate thawing due to shading-induced cooling (Blok et al., 2010). A warmer climate can also affect N cycling by changing N mineralization rates (Wårlind et al., 2014). However, the extent to which warming and permafrost thaw can alleviate nutrient limitation in high-latitude cold soils and how this might affect vegetation dynamics remains unclear. Despite biogeochemical feedbacks beyond the scope of this study, they are strongly related to the effects of BF on terrestrial C cycle (Zhang et al., 2014). In an analysis of RCA-GUESS simulations with and without BF to climate following the RCP8.5 forcing scenario, Zhang et al. (2014) found that terrestrial ecosystems in the Arctic tundra and boreal forests will act as C sinks in the coming century. However, simulations with BF enabled sequestered more C, with an additional uptake of 8.5 Gt C, or 22% of the total C sink, over the century. All these aspects are essential to our understanding of BF in modulating the magnitude and seasonality of climate change and will be assessed in future studies with RCA-GUESS and the EC-Earth ESM, both of which have recently been coupled to LPJ-GUESS version 4 (Smith et al., 2014) which includes N limitations on plant productivity and C-N dynamics in soils (Wårlind et al., 2014).

This study sheds new light on the joint evolution of vegetation and climate over boreal and Arctic regions, attributing the simulated variations to underlying mechanisms in a detailed way. It is also a first study to use a fully coupled regional Earth system model to assess the effects of BF at different levels of radiative

forcing. We conclude that BF of vegetation changes are likely to amplify Arctic warming and, in a stronger radiative forcing scenario, lead to a longer, more thermally equitable growing season, as well as enhancing the mean and variability of growing-season precipitation. Such shifts in the physical conditions experienced by Arctic ecosystems during the critical season for vegetation activity are conducive to a continuation and enhancement of ecological trends already being experienced across the Arctic, including the increased productivity, stature and density of vegetation, a poleward advance of the boreal forest tree-line, and a competitive shift favoring the woody elements of arctic vegetation.

Acknowledgments

This work was performed as part of the project Advanced Simulation of Arctic Climate and Impact on Northern Regions (ADSIMNOR), funded by the Swedish Research Council FORMAS. We thank Martin Jung who kindly contributed the upscaled LHF data set. The study is a contribution to the strategic research areas Modeling the Regional and Global Earth System (MERGE) and Biodiversity and Ecosystem Services in a Changing Climate (BECC), the Lund University Centre for Studies of Carbon Cycle and Climate Interactions (LUCCI), and the Nordic Centre of Excellence (DEFROST). All the data sets used in this study are available in <https://doi.org/10.6084/m9.figshare.5960881.v1> and <https://dataguru.lu.se/>. J. Mao is supported by the Reducing Uncertainties in Biogeochemical Interactions through Synthesis and Computing Scientific Focus Area (RUBISCO SFA), which is sponsored by the Regional and Global Climate Modeling (RGCM) Program in the Climate and Environmental Sciences Division (CESD) of the Biological and Environmental Research (BER) Program in the U.S. Department of Energy Office of Science. Oak Ridge National Laboratory is managed by UT-BATTELLE for DOE under contract DE-AC05-00OR22725.

References

- ACIA (2005). *Arctic climate impact assessment* (p. 1042). Cambridge, UK: Cambridge University Press.
- Alkama, R., & Cescatti, A. (2016). Biophysical climate impacts of recent changes in global forest cover. *Science*, *351*(6273), 600–604. <https://doi.org/10.1126/science.aac8083>
- Beringer, J., Chapin Iii, F. S., Thompson, C. C., & McGuire, A. D. (2005). Surface energy exchanges along a tundra-forest transition and feedbacks to climate. *Agricultural and Forest Meteorology*, *131*(3–4), 143–161. <https://doi.org/10.1016/j.agrformet.2005.05.006>
- Berner, L. T., Beck, P. S. A., Bunn, A. G., & Goetz, S. J. (2013). Plant response to climate change along the forest-tundra ecotone in northeastern Siberia. *Global Change Biology*, *19*(11), 3449–3462.
- Bintanja, R., & Selten, F. M. (2014). Future increases in Arctic precipitation linked to local evaporation and sea-ice retreat. *Nature*, *509*(7501), 479–482. <https://doi.org/10.1038/nature13259>
- Blok, D., Heijmans, M. M. P. D., Schaepman-Strub, G., Kononov, A. V., Maximov, T. C., & Berendse, F. (2010). Shrub expansion may reduce summer permafrost thaw in Siberian tundra. *Global Change Biology*, *16*(4), 1296–1305. <https://doi.org/10.1111/j.1365-2486.2009.02110.x>
- Bonan, G. B. (2008). Forests and climate change: Forcings, feedbacks, and the climate benefits of forests. *Science*, *320*(5882), 1444–1449. <https://doi.org/10.1126/science.1155121>
- Bond-Lamberty, B. (2013). Global vegetation model diversity and the risks of climate-driven ecosystem shifts. *Environmental Research Letters*, *8*(4), 041004. <https://doi.org/10.1088/1748-9326/8/4/041004>
- Bonfils, C. J. W., Phillips, T. J., Lawrence, D. M., Cameron-Smith, P., Riley, W. J., & Subin, Z. M. (2012). On the influence of shrub height and expansion on northern high latitude climate. *Environmental Research Letters*, *7*(1), 015503. <https://doi.org/10.1088/1748-9326/7/1/015503>
- Chapin, F. S., Sturm, M., Serreze, M. C., McFadden, J. P., Key, J. R., Lloyd, A. H., et al. (2005). Role of land-surface changes in Arctic summer warming. *Science*, *310*(5748), 657–660. <https://doi.org/10.1126/science.1117368>
- Claussen, M., Fohlmeister, J., Ganopolski, A., & Brovkin, V. (2006). Vegetation dynamics amplifies precessional forcing. *Geophysical Research Letters*, *33*, L09709. <https://doi.org/10.1029/2006GL026111>
- De Wit, H. A., Bryn, A., Hofgaard, A., Karstensen, J., Kvalevåg, M. M., & Peters, G. P. (2014). Climate warming feedback from mountain birch forest expansion: Reduced albedo dominates carbon uptake. *Global Change Biology*, *20*(7), 2344–2355. <https://doi.org/10.1111/gcb.12483>
- Dekker, S. C., de Boer, H. J., Brovkin, V., Fraedrich, K., Wassen, M. J., & Rietkerk, M. (2010). Biogeophysical feedbacks trigger shifts in the modelled vegetation-atmosphere system at multiple scales. *Biogeosciences*, *7*(4), 1237–1245. <https://doi.org/10.5194/bg-7-1237-2010>
- Dirmeyer, P. A., Jin, Y., Singh, B., & Yan, X. (2013). Trends in land-atmosphere interactions from CMIP5 simulations. *Journal of Hydrometeorology*, *14*(3), 829–849. <https://doi.org/10.1175/JHM-D-12-0107.1>
- Elmendorf, S. C., Henry, G. H. R., Hollister, R. D., Björk, R. G., Björkman, A. D., Callaghan, T. V., et al. (2012). Global assessment of experimental climate warming on tundra vegetation: Heterogeneity over space and time. *Ecology Letters*, *15*(2), 164–175. <https://doi.org/10.1111/j.1461-0248.2011.01716.x>
- Euskirchen, E. S., McGuire, A. D., Chapin, F. S., Yi, S., & Thompson, C. C. (2009). Changes in vegetation in northern Alaska under scenarios of climate change, 2003–2100: Implications for climate feedbacks. *Ecological Applications*, *19*(4), 1022–1043. <https://doi.org/10.1890/08-0806.1>
- Green, J. K., Konings, A. G., Alemohammad, S. H., Berry, J., Entekhabi, D., Kolassa, J., et al. (2017). Regionally strong feedbacks between the atmosphere and terrestrial biosphere. *Nature Geoscience*, *10*, 410–414.
- Göttel, H., Alexander, J., Keup-Thiel, E., Rechid, D., Hagemann, S., Blome, T., et al. (2008). Influence of changed vegetations fields on regional climate simulations in the Barents Sea region. *Climate Change*, *87*(1–2), 35–50. <https://doi.org/10.1007/s10584-007-9341-5>
- Hazeleger, W., Wang, X., Severijns, C., Ştefănescu, S., Bintanja, R., Sterl, A., et al. (2012). EC-Earth V2.2: Description and validation of a new seamless Earth system prediction model. *Climate Change*, *39*, 2611–2629.
- Jung, M., Reichstein, M., Margolis, H. A., Cescatti, A., Richardson, A. D., Arain, M. A., et al. (2011). Global patterns of land-atmosphere fluxes of carbon dioxide, latent heat, and sensible heat derived from eddy covariance, satellite, and meteorological observations. *Journal of Geophysical Research*, *116*, G00J07. <https://doi.org/10.1029/2010JG001566>
- Kasurinen, V., Alfredsen, K., Kolari, P., Mammarella, I., Alekseychik, P., Rinne, J., et al. (2014). Latent heat exchange in the boreal and arctic biomes. *Global Change Biology*, *20*(11), 3439–3456. <https://doi.org/10.1111/gcb.12640>
- Kjellström, E., Bärring, L., Gollvik, S., Hansson, U., Jones, C., Samuelsson, P., et al. (2005). A 140-year simulation of European climate with the new version of the Rossby Centre regional atmospheric climate model (RCA3). *SMHI Reports Meteorology and Climatology*, *108*, SMHI, SE-60176.
- Kueppers, L. M., Snyder, M. A., Sloan, L. C., Zavaleta, E. S., & Fulfrost, B. (2005). Modeled regional climate change and California endemic oak ranges. *Proceedings of the National Academy of Sciences of the United States of America*, *102*(45), 16,281–16,286. <https://doi.org/10.1073/pnas.0501427102>
- Lawrence, D. M., Koven, C. D., Swenson, S. C., Riley, W. J., & Slater, A. G. (2015). Permafrost thaw and resulting soil moisture changes regulate projected high-latitude CO₂ and CH₄ emissions. *Environmental Research Letters*, *10*(9), 094011. <https://doi.org/10.1088/1748-9326/10/9/094011>
- Lawrence, D. M., & Swenson, S. C. (2011). Permafrost response to increasing Arctic shrub abundance depends on the relative influence of shrubs on local soil cooling versus large-scale climate warming. *Environmental Research Letters*, *6*(4), 045504. <https://doi.org/10.1088/1748-9326/6/4/045504>
- Li, Y., Zhao, M., Motesarrei, S., Mu, Q., Kalnay, E., & Li, S. (2015). Local cooling and warming effects of forests based on satellite observations. *Nature Communications*, *6*(1), 6603. <https://doi.org/10.1038/ncomms7603>
- Lorantny, M. M., Berner, L. T., Goetz, S. J., Jin, Y., & Randerson, J. T. (2013). Vegetation controls on northern high latitude snow-albedo feedback: Observations and CMIP5 model predictions. *Global Change Biology*, *20*(2), 594–606.

- Matthes, H., Rinke, A., Miller, P., Kuhry, P., Dethloff, K., & Wolf, A. (2012). Sensitivity of high-resolution Arctic regional climate model projections to different implementations of land surface processes. *Climate Change*, *111*(2), 197–214. <https://doi.org/10.1007/s10584-011-0138-1>
- Mitchell, T. D., & Jones, P. D. (2005). An improved method of constructing a database of monthly climate observations and associated high-resolution grids. *International Journal of Climatology*, *25*(6), 693–712. <https://doi.org/10.1002/joc.1181>
- Muller, J. P., López, G., Watson, G., Shane, N., Kennedy, T., Yuen, P., et al. (2012). The ESA GlobAlbedo Project for mapping the Earth's land surface albedo for 15 years from European sensors, IEEE Geoscience and Remote Sensing Symposium (IGARSS) 2012, IEEE, Munich, Germany, 22-27.7.12.
- Pearson, R. G., Phillips, S. J., Lorant, M. M., Beck, P. S. A., Damoulas, T., Knight, S. J., & Goetz, S. J. (2013). Shifts in Arctic vegetation and associated feedbacks under climate change. *Nature Climate Change*, *3*(7), 673–677. <https://doi.org/10.1038/nclimate1858>
- Ramankutty, N., Foley, J. A., Hall, F. G., Collatz, G. J., Meeson, B. W., Los, S. O., et al. (2010). ISLSCP II potential natural vegetation cover. ORNL DAAC, Oak Ridge, Tennessee, USA.
- Samuelsson, P., Gollvik, S., Jansson, C., Kupiainen, M., Kourzeneva, E., & van de Berg, W. J. (2015). The surface processes of the Rossby Centre regional atmospheric climate model (RCA4). SMHI Rep. 157 (58 pp.).
- Samuelsson, P., Jones, C. G., Willén, U., Ullerstig, A., Gollvik, S., Hansson, U. L. F., et al. (2011). The Rossby Centre regional climate model RCA3: Model description and performance. *Tellus A*, *63*(1), 4–23. <https://doi.org/10.1111/j.1600-0870.2010.00478.x>
- Seddon, A. W. R., Macias-Fauria, M., Long, P. R., Benz, D., & Willis, K. J. (2016). Sensitivity of global terrestrial ecosystems to climate variability. *Nature*, *531*(7593), 229–232. <https://doi.org/10.1038/nature16986>
- Smith, B., Prentice, I. C., & Sykes, M. T. (2001). Representation of vegetation dynamics in the modelling of terrestrial ecosystems: Comparing two contrasting approaches within European climate space. *Global Ecology and Biogeography*, *10*(6), 621–637. <https://doi.org/10.1046/j.1466-822X.2001.00256.x>
- Smith, B., Samuelsson, P., Wramneby, A., & Rummukainen, M. (2011). A model of the coupled dynamics of climate, vegetation and terrestrial ecosystem biogeochemistry for regional applications. *Tellus A*, *63*(1), 87–106. <https://doi.org/10.1111/j.1600-0870.2010.00477.x>
- Smith, B., Wärlind, D., Arneth, A., Hickler, T., Leadley, P., Siltberg, J., & Zaehle, S. (2014). Implications of incorporating N cycling and N limitations on primary production in an individual-based dynamic vegetation model. *Biogeosciences*, *11*, 2027–2054.
- Stiegler, C., Lund, M., Christensen, T. R., Mastepanov, M., & Lindroth, A. (2016). Two years with extreme and little snowfall: Effects on energy partitioning and surface energy exchange in a high-Arctic tundra ecosystem. *The Cryosphere*, *10*(4), 1395–1413. <https://doi.org/10.5194/tc-10-1395-2016>
- Stocker, T., Qin, D., Plattner, G.-K., Tignor, M., Allen, S. K., Boschung, J., et al. (Eds.) (2013). *Climate change 2013: The physical science basis. Contribution of working group I to the fifth assessment report of the intergovernmental panel on climate change*. Cambridge, UK, and New York: Cambridge University Press.
- Swann, A. L., Fung, I. Y., Levis, S., Bonan, G. B., & Doney, S. C. (2010). Changes in Arctic vegetation amplify high-latitude warming through the greenhouse effect. *Proceedings of the National Academy of Sciences of the United States of America*, *107*(4), 1295–1300. <https://doi.org/10.1073/pnas.0913846107>
- Tape, K. E. N., Sturm, M., & Racine, C. (2006). The evidence for shrub expansion in Northern Alaska and the Pan-Arctic. *Global Change Biology*, *12*(4), 686–702. <https://doi.org/10.1111/j.1365-2486.2006.01128.x>
- Undén, P., Rontu, L., Järvinen, H., Lynch, P., Calvo, J., Cats, G., et al. (2002). HIRLAM-5 scientific documentation, Tech. Rep., Swedish Meteorological and Hydrological Institute, S-601 76 Norrköping, Sweden.
- Wärlind, D., Smith, B., Hickler, T., & Arneth, A. (2014). Nitrogen feedbacks increase future terrestrial ecosystem carbon uptake in an individual-based dynamic vegetation model. *Biogeosciences*, *11*(21), 6131–6146. <https://doi.org/10.5194/bg-11-6131-2014>
- Willeit, M., Ganopolski, A., & Feulner, G. (2014). Asymmetry and uncertainties in biogeophysical climate–vegetation feedback over a range of CO₂ forcings. *Biogeosciences*, *11*(1), 17–32. <https://doi.org/10.5194/bg-11-17-2014>
- Wramneby, A., Smith, B., & Samuelsson, P. (2010). Hot spots of vegetation–climate feedbacks under future greenhouse forcing in Europe. *Journal of Geophysical Research*, *115*, D21119. <https://doi.org/10.1029/2010JD014307>
- Wyser, K., Jones, C. G., Gu, P., Girard, E., Willén, U., Cassano, J., et al. (2008). An evaluation of Arctic cloud and radiation processes during the SHEBA year: Simulation results from eight Arctic regional climate models. *Climate Dynamics*, *30*(2-3), 203–223. <https://doi.org/10.1007/s00382-007-0286-1>
- Zhang, J., & Walsh, J. E. (2006). Thermodynamic and hydrological impacts of increasing greenness in northern high latitudes. *Journal of Hydrometeorology*, *7*(5), 1147–1163. <https://doi.org/10.1175/JHM535.1>
- Zhang, W., Jansson, C., Miller, P. A., Smith, B., & Samuelsson, P. (2014). Biogeophysical feedbacks enhance the Arctic terrestrial carbon sink in regional Earth system dynamics. *Biogeosciences*, *11*(19), 5503–5519. <https://doi.org/10.5194/bg-11-5503-2014>
- Zhang, W., Miller, P. A., Smith, B., Wania, R., Koenig, T., & Döscher, R. (2013). Tundra shrubification and tree-line advance amplify arctic climate warming: Results from an individual-based dynamic vegetation model. *Environmental Research Letters*, *8*(3), 034023. <https://doi.org/10.1088/1748-9326/8/3/034023>